Performance and field tests of a handheld Compton camera using 3-D position-sensitive scintillators coupled to multi-pixel photon counter arrays

2014 JINST 9 P11025

(http://iopscience.iop.org/1748-0221/9/11/P11025)

PUBLISHED BY IOP PUBLISHING FOR SISSA MEDIALAB

RECEIVED: *July 15, 2014*
REVISED: *October 23, 2014*
ACCEPTED: *November 10, 2014*
PUBLISHED: *November 27, 2014*

Performance and field tests of a handheld Compton camera using 3-D position-sensitive scintillators coupled to multi-pixel photon counter arrays

A. Kishimoto,[a,1] **J. Kataoka,**[a] **T. Nishiyama,**[a] **T. Fujita,**[a] **K. Takeuchi,**[a] **H. Okochi,**[a] **H. Ogata,**[a] **H. Kuroshima,**[a] **S. Ohsuka,**[b] **S. Nakamura,**[c] **M. Hirayanagi,**[c] **S. Adachi,**[c] **T. Uchiyama**[c] **and H. Suzuki**[c]

[a] *Research Institute for Science and Engineering, Waseda University, 3-4-1 Okubo, Shinjuku, Tokyo, 169-8555, Japan*
[b] *Central Research Laboratory, Hamamatsu Photonics K.K., 5000, Hirakuchi, Hamakita-ku, Hamamatsu, Shizuoka, Japan*
[c] *Hamamatsu Photonics K.K., 1126-1, Ichino-cho, Higashi-ku, Hamamatsu, Shizuoka, Japan*

E-mail: daphne3h-aya@y.ruri.waseda.jp

ABSTRACT: After the nuclear disaster in Fukushima, radiation decontamination has become particularly urgent. To help identify radiation hotspots and ensure effective decontamination operation, we have developed a novel Compton camera based on Ce-doped $Gd_3Al_2Ga_3O_{12}$ scintillators and multi-pixel photon counter (MPPC) arrays. Even though its sensitivity is several times better than that of other cameras being tested in Fukushima, we introduce a depth-of-interaction (DOI) method to further improve the angular resolution. For gamma rays, the DOI information, in addition to 2-D position, is obtained by measuring the pulse-height ratio of the MPPC arrays coupled to ends of the scintillator. We present the detailed performance and results of various field tests conducted in Fukushima with the prototype 2-D and DOI Compton cameras. Moreover, we demonstrate stereo measurement of gamma rays that enables measurement of not only direction but also approximate distance to radioactive hotspots.

KEYWORDS: Compton imaging; Gamma detectors (scintillators, CZT, HPG, HgI etc)

[1] Corresponding author.

doi:10.1088/1748-0221/9/11/P11025

2014 JINST 9 P11025

Contents

2014 JINST 9 P11025

1 Introduction

After the Japanese nuclear disaster in 2011, a large number of radioactive isotopes were released, and the residual radiation remains a serious problem in Fukushima. To identify radiation hotspots, various gamma cameras have been developed such as the Compton camera [1]. A Compton camera utilizes the kinematics of Compton scattering to construct a source image, does not require mechanical collimators or coded masks, and features a wide field of view (FOV). For example, the Si/CdTe Compton camera [2], which is a key technology of the Soft Gamma-ray Detector for Japan's sixth X-ray astronomy mission (Astro-H) [3], featured excellent angular resolution. However, the poor sensitivity of semiconductor devices to high-energy gamma rays, such as ^{137}Cs (662 keV) and ^{134}Cs (605 keV, 796 keV), requires a long data acquisition time to reconstruct an image. Alternatively, various semiconductor detectors have been utilized in Compton cameras [4–6].

In this study, we significantly improve the detection efficiency using inorganic scintillators. In fact, several two-plane Compton cameras consisting of scintillating materials have already been proposed for medical imaging and security investigations [7, 8]. Despite the high detection efficiency, the resolution of scintillator-based Compton cameras tends to be lower than those based on semiconductor detectors due to the poor position and energy resolution of the scintillating detectors. We present a novel Compton camera [9, 10] that applies the method of 3-D position measurement in scintillator blocks, significantly improving the trade-off between efficiency and resolution. This study describes the conceptual design and basic performance of our Compton camera as well as the results of field tests conducted with the camera in Fukushima.

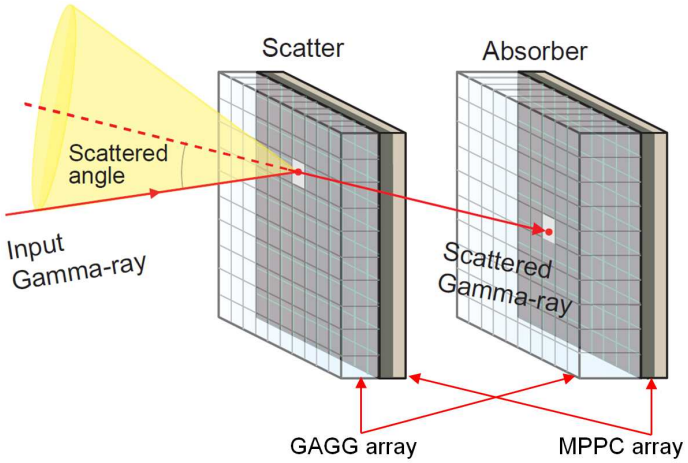

Figure 1. Conceptual design of the two-plane Compton camera.

2 Handheld Compton camera

2.1 Principle and concept of our Compton camera

The arrival direction of an incident gamma-ray is calculated using the position and energy information in two detectors: scatterer and absorber (figure 1). The scatterering angle is calculated from the measured information as follows:

$$cos\theta_E = 1 - \frac{m_e c^2}{E_2} + \frac{m_e c^2}{E_1 + E_2} \tag{2.1}$$

where E_1 denotes the energy of the recoil electron and E_2 describes the energy of the scattered photon. The Compton camera resolution is usually presented by the distribution of the angular resolution measure (ARM), which is defined as follows:

$$\mathrm{ARM} \equiv \theta_E - \theta_G \tag{2.2}$$

where θ_E is the scattering angle as calculated from the measured energy information [given by eq. (2.1)], and θ_G is calculated from geometrical information obtained by gamma-ray interaction positions and the source position. The geometrical contribution to the angular resolution largely depends on the 3-D position resolution of the gamma interaction in both detectors, which is related to the thickness of the scintillator, and on the distance between the scatterer and absorber. With regard to efficiency, a small distance between the detectors and a thick scintillator are preferable, especially for the measurement of high-energy gamma rays, but these configurations can lead to a large fluctuation in θ_G. Accordingly, by measuring the depth-of-interaction (DOI) information, the angular resolution can be improved at a close distance, thereby achieving good angular resolution and efficiency simultaneously. Figure 2 shows the variation of angular resolution calculated by Geant4 simulation as a function of distance for both the DOI and non-DOI configurations. The figure clearly shows the benefit of measuring DOI on the angular resolution [9].

2014 JINST 9 P11025

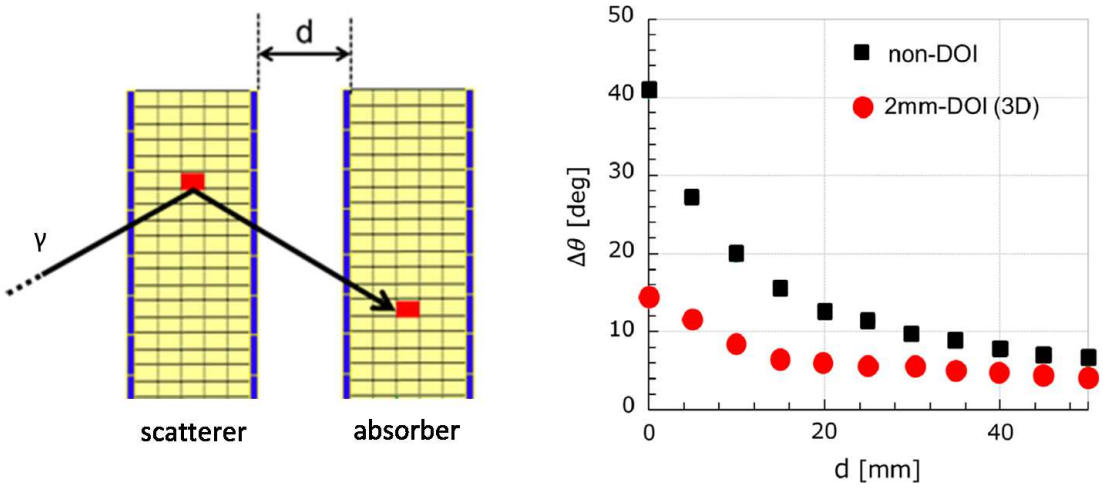

Figure 2. Variation of the angular resolution $\Delta\theta$ as a function of distance d for the DOI and non-DOI configurations. This figure is calculated using Geant4 simulation, assuming $50 \times 50\,\mathrm{mm}^2$ Ce:GAGG scintillator plates with 10-mm thickness for both the scatterer and the absorber.

2.2 Configuration of the Compton camera

Figure 3(a) shows the detector configuration and figure 3(b) shows the block diagram of our Compton camera system. The Compton camera is small in size $(14 \times 15 \times 15\,\mathrm{cm}^3)$ and lightweight (1.9 kg) [9, 11]. The camera consists of a gamma-ray detection unit together with an optical fish-eye camera, a signal processing unit, and a USB 3.0 interface for accumulating data on a personal computer. In the gamma-ray detection unit, we use Ce-doped $Gd_3Al_2Ga_3O_{12}$ (Ce:GAGG) scintillators [12] and 8×8 large monolithic multi-pixel photon counter (MPPC) arrays [13–15]. Signals from these MPPC arrays are passed through a resistive charge-division network [11, 16] and are then fed into a signal-processing unit. The signal-processing unit consists of an application-specific integrated circuit (ASIC), analog-to-digital converter (ADC), programmable logic device (PLD), and a high-voltage power supply (HVPS). The ASIC includes a pulse-shaping amplifier, baseline restorer circuit, comparator circuit, and peak-hold circuit. The HVPS includes a temperature-compensating function that can automatically adjust the bias voltage to ambient temperature around the MPPCs.

For this study, we fabricated two types of Compton cameras in conjunction with Hamamatsu Photonics K. K.: the 2-D mode (non-DOI) and 3-D mode (DOI) Compton cameras. Both the non-DOI and DOI Compton cameras consist of Ce:GAGG scintillator arrays; table 1 lists the detailed scintillator configuration. In the DOI Compton camera, the scatterer and absorber are divided into layers. Each layer of the scatterer is coupled to the MPPC array, and the signals are read out layer-by-layer. In contrast, the absorber of the DOI Compton camera uses 3-D position-sensitive scintillators [17]. We can determine the DOI of incident gamma rays by measuring the pulse-height ratio of dual-sided MPPC arrays coupled to the ends of the absorber. An enhanced specular reflector (ESR) divides each pixel of the crystal block in the x- and y-direction, whereas a layer of air separates the crystals in the DOI direction or z-direction. The x, y and z (=DOI) interaction positions are calculated by applying the centroid method to the eight signals output via the resistor network.

2014 JINST 9 P11025

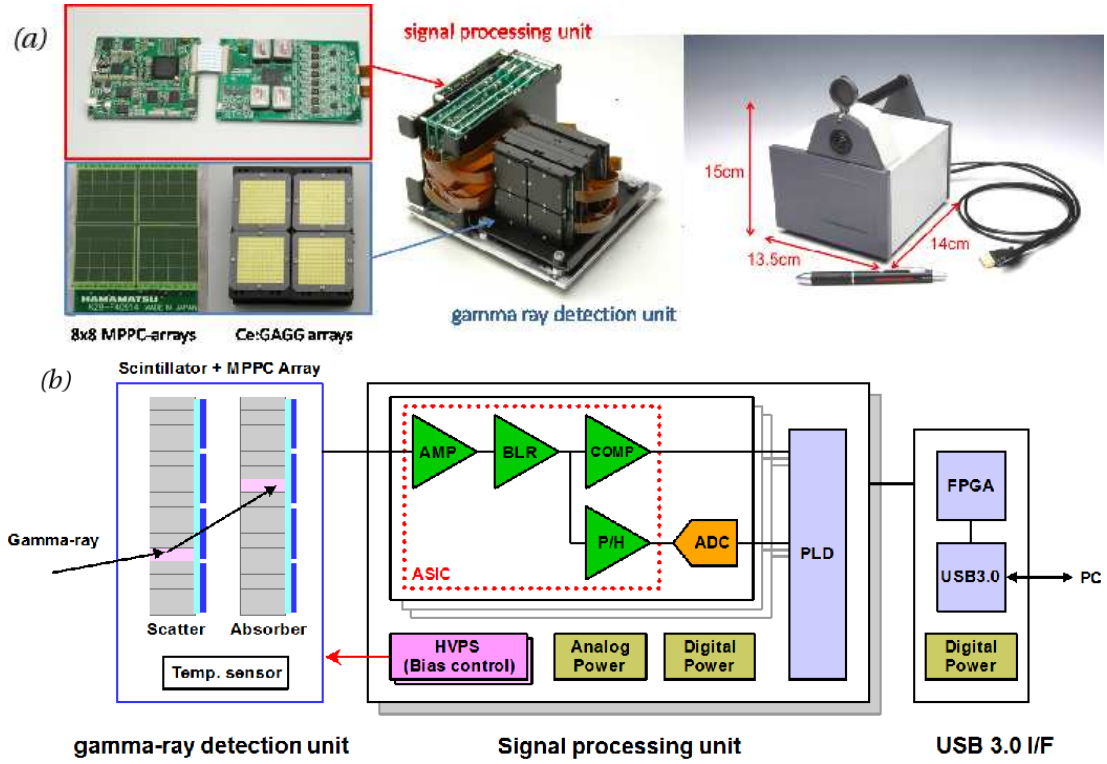

Figure 3. (a) Photograph of the internal components of the DOI Compton camera as well as the dimensions of the external housing. (b) Read-out diagram of the Compton camera developed in this study.

3 Basic performance

3.1 Non-DOI Compton camera

First, we evaluate the performance of the 2-D mode (non-DOI) Compton camera. Figure 4 shows 1-D and 2-D energy spectra, while figure 5 shows the maximum-likelihood expectation-maximization (ML-EM) image of ^{137}Cs measurement. We measured a 10 MBq point source at a distance of 50 cm ($\sim 5\,\mu$Sv/h) with an acquisition time of 30 sec. The average energy resolution was 9% (FWHM) at 662 keV. The hotspot in figure 4(b) reflects back-scattering events, that is, events that are first scattered in the absorber and then absorbed in the scatterer. In reconstructing the gamma-ray distribution images, we select events using the following criteria to remove background and noise events such as back-scattering: $10\,\mathrm{keV} \leq E_{\mathrm{scat}} \leq 165\,\mathrm{keV}$ and $612\,\mathrm{keV} \leq E_{\mathrm{tot}} \leq 712\,\mathrm{keV}$. Here, E_{scat} and E_{tot} denote the energy deposit in the scatterer and the total energy, which is the sum of energy deposits in both the scatterer and absorber, respectively. In the non-DOI camera configuration, we achieve an angular resolution of $\Delta\theta \sim 14^{\circ}$ (FWHM), which is calculated from the ARM distribution.

In our Compton camera, the simple back-projection (SBP) image and the ML-EM image are updated every second by integrating the accumulated data over an arbitrary time. We have confirmed that a typical acquisition time of 20 to 30 seconds is required to reconstruct images in an environment of about 5 μSv/h. Thus, we demonstrated that, due to high-efficiency, real-time imaging is possible.

2014 JINST 9 P11025

Table 1. Scintillator configuration for the non-DOI and DOI Compton cameras. Here, *Array* denotes scintillators coupled to an MPPC array, and *Assembly* denotes the combination of a scintillator array and an MPPC array.

Parameter	Value
non-DOI	
SCATTERER	
Pixel size	$1.5 \times 1.5 \times 5.0\,\mathrm{mm}^3$
Array configuration	15×15 pixels, 4 blocks
Layer	1 layer
Assembly	1
ABSORBER	
Pixel size	$1.5 \times 1.5 \times 10.0\,\mathrm{mm}^3$
Array configuration	15×15 pixels, 4 blocks
Layer	1 layer
Assembly	1
DISTANCE	16 mm
DOI	
SCATTERER	
Pixel size	$2.0 \times 2.0 \times 4.0\,\mathrm{mm}^3$
Array configuration	11×11 pixels, 4 blocks
Layer	2 layers
Assembly	2
ABSORBER	
Pixel size	$2.0 \times 2.0 \times 2.0\,\mathrm{mm}^3$
Array configuration	$11 \times 11 \times 10$ pixels, 4 blocks
Layer	10 layers
Assembly	1
DISTANCE	12 mm

3.2 DOI Compton camera

Next, we evaluate the basic properties of the 3-D mode (DOI) Compton camera. Figure 6 shows the position response in a performance test for the 3-D position-sensitive scintillator of the Compton camera as measured for 662 keV gamma rays. Figure 6(b) shows the pulse-height diagram collected at the scintillator block ends, which clearly distinguishes the crystal responses of each layer. From figure 6, we can confirm that the gamma-ray interaction position in the scintillator block is determined three-dimensionally with an accuracy of 2 mm. The average energy resolution of the 3-D position-sensitive scintillator is 8.6% at 662 keV.

Figure 7 shows the ML-EM images of a ^{137}Cs point source obtained under various source configurations, including (1) $(\theta,\phi) = (+45^\circ, 0^\circ)$, (2) $(\theta,\phi) = (0^\circ, 0^\circ)$ (center of the field of view), and (3) $(\theta,\phi) = (-45^\circ, 0^\circ)$. The source intensity and distance are 10 MBq and 140 cm, respectively, which equals $\sim 0.5\,\mu$Sv/h, with an acquisition time of 1 min for each datum point. The images correctly reflect each source position, and the angular resolutions are (1) 7.9° (FWHM),

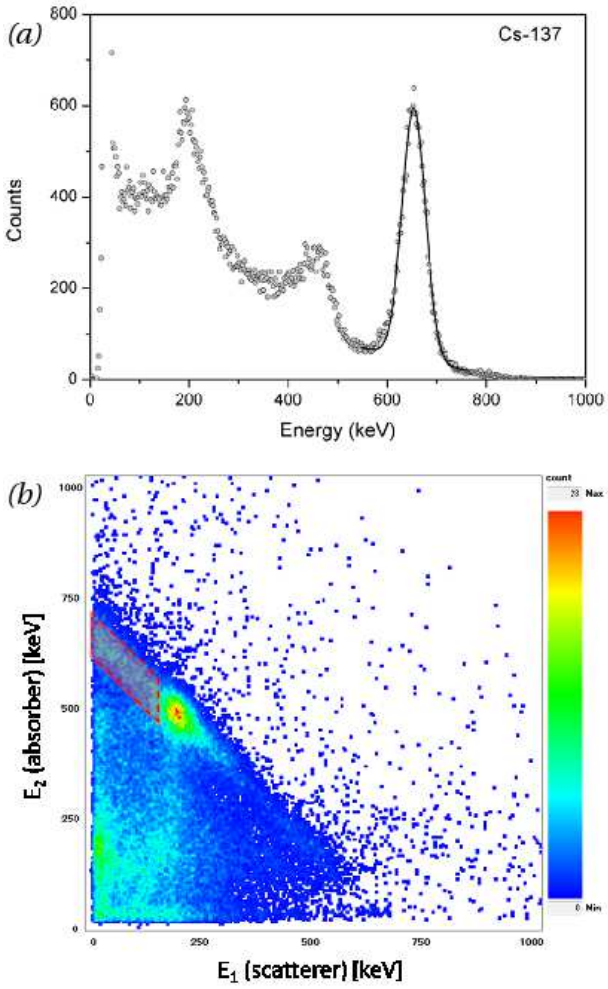

Figure 4. (a) The 1-D (energy sum) and (b) 2-D (E_{absorber} vs. $E_{\text{scatterer}}$) energy spectra of the non-DOI Compton camera. The average energy resolution is 9% (FWHM) at 662 keV. The highlighted parallelogram in the 2-D energy spectrum represents the cuts used for gamma-ray image reconstruction.

(2) 8.8° (FWHM), and (3) 8.7° (FWHM). Figure 8 shows an example of the ARM distribution for the non-DOI and DOI Compton cameras. The ARM distribution of DOI camera is clearly improved compared to that of non-DOI camera.

In fact, we have clearly resolved two sources that are separated by 10°. Figure 9 shows the ML-EM images of two ^{137}Cs point sources obtained with the non-DOI and DOI Compton cameras. The two point sources cannot be separated in the non-DOI image but are clearly resolved in the DOI image. This result shows that the DOI camera significantly improves the angular resolution. Moreover, the efficiency of the DOI Compton camera was 1.5–2 times higher than that of the non-DOI camera due to the increased thickness of the detector and smaller distance between the scatterer and absorber. Figure 10 shows the intrinsic efficiency obtained by Geant4 simulation and a comparison to the experimental values as a function of source position $|\theta|$ (at $\phi = 0°$). The intrinsic efficiency of the DOI Compton camera is $0.43 \pm 0.019\%$ at $|\theta| = 0°$ and $0.23 \pm 0.018\%$ at $|\theta| = 45°$. These values are very consistent with the simulation, suggesting high detection performance.

2014 JINST 9 P11025

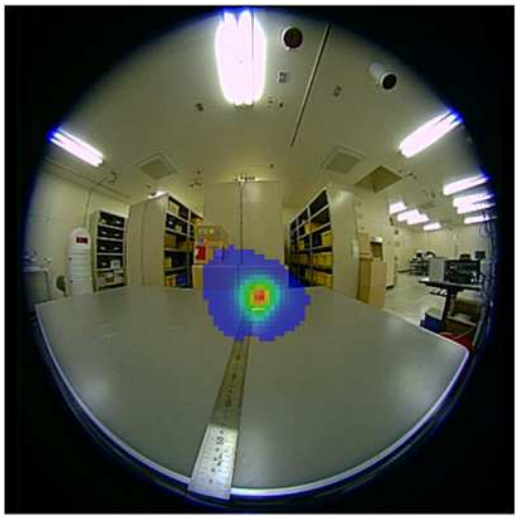

Figure 5. The ML-EM image of the ^{137}Cs point source measurement taken using the non-DOI Compton camera, superimposed on the optical fish-eye image. The calculated angular resolution $\Delta\theta$ is 14° (FWHM).

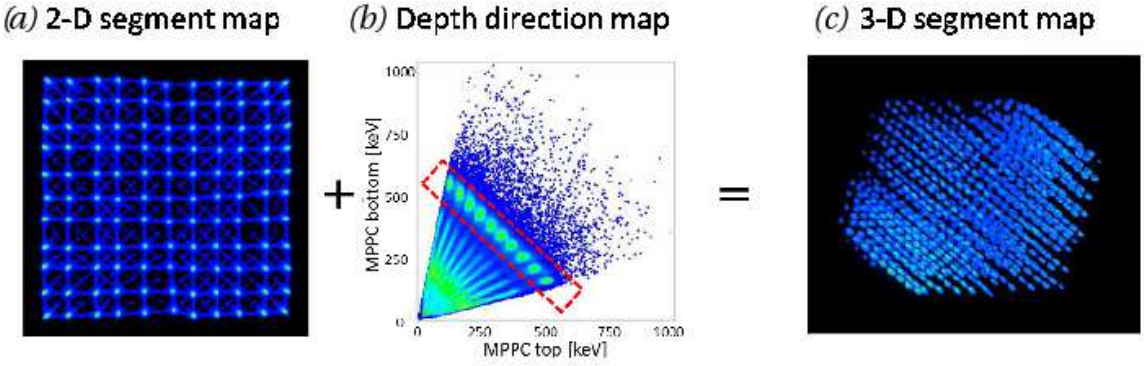

Figure 6. (a) The 2-D segment map and (b) depth direction map used for generating the 3-D segment map. The horizontal axis is used for the pulse-height of the top MPPC array, while the vertical axis is used for that of the bottom MPPC array. The line in (b) denotes the position of the photoelectric peak. (c) The 3-D segment map of each 2-mm cubic Ce:GAGG scintillator as measured for 662 keV gamma rays.

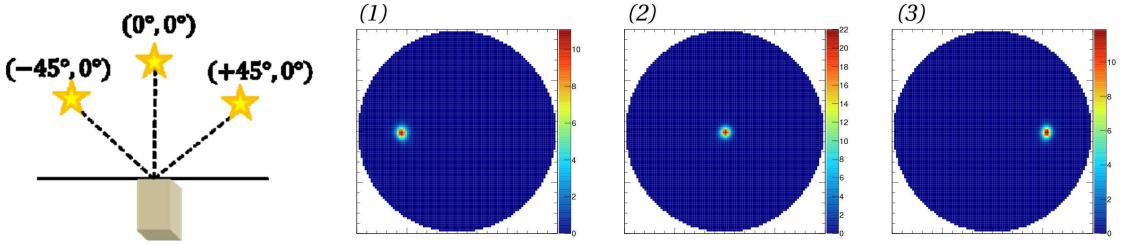

Figure 7. The ML-EM images taken by the DOI Compton camera under the following source configurations: (1) $(\theta,\phi) = (+45^\circ, 0^\circ)$, (2) $(\theta,\phi) = (0^\circ, 0^\circ)$, and (3) $(\theta,\phi) = (-45^\circ, 0^\circ)$. All source distances are 140 cm.

2014 JINST 9 P11025

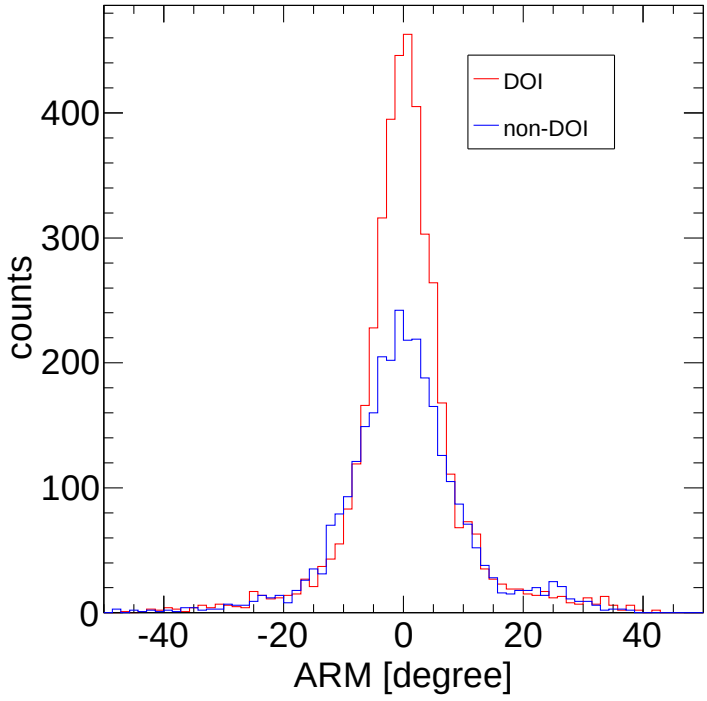

Figure 8. The ARM distribution for the non-DOI and DOI Compton cameras at the source configuration of $\theta = 0^\circ$ [position (2) in figure 7]. The acquisition time for both cameras is 30 min.

4 Field tests in Fukushima

The non-DOI and DOI Compton cameras have been tested several times in Namie, Fukushima. Figure 11(a) shows an example image acquired by the non-DOI Compton camera during field tests conducted in May 2013. The brightest hotspots (shown in red) in the image correspond to $\sim 50\,\mu$Sv/h when measured with a survey meter at a distance of 1 cm. Figure 11(b) shows an image collected by the DOI camera in July 2014. From figure 11(b), we can confirm that the hotspot distribution spreads along the path and that the dose level of the bush adjacent to the forest path is higher than that of the path. The dose rate at the camera was $\sim 4\,\mu$Sv/h, and the brightest hotspot corresponds to $\sim 10\,\mu$Sv/h. Both figure 11(a) and 11(b) show SBP images with an acquisition time of 3 min. We confirmed that these images accurately reflected the position of hotspots.

Figure 12 shows the 1-D energy spectrum calculated from energy deposits in the scatterer and absorber collected by the DOI camera during the image acquisition shown in figure 11(b). Three photoelectric peaks clearly appear at 662 keV (^{137}Cs), 605 keV, and 796 keV (^{134}Cs). From this energy spectrum, we selected only the events corresponding to ^{137}Cs by setting an energy range: $612\,\text{keV} \leq E_{\text{tot}} \leq 712\,\text{keV}$ and $10\,\text{keV} \leq E_{\text{scat}} \leq 165\,\text{keV}$. By changing the energy range, we can also acquire the ^{134}Cs distribution.

Through these field tests, we have confirmed that radiation hotspot images can typically be acquired in 5–10 min, even with background contamination of $5\,\mu$Sv/h.

2014 JINST 9 P11025

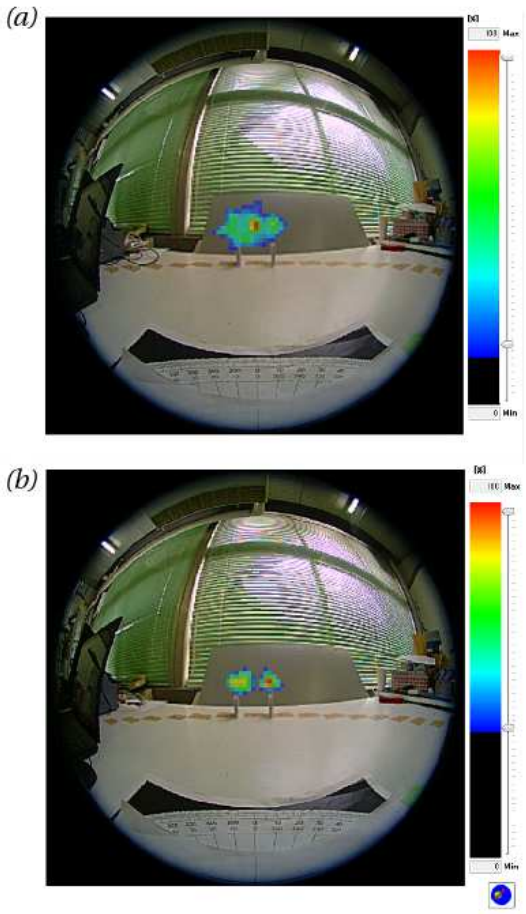

Figure 9. The ML-EM images of two ^{137}Cs point sources separated by an angle of 10° acquired by (a) the non-DOI Compton camera and (b) the DOI Compton camera.

5 Stereo application

While the Compton camera can provide useful gamma-ray images, uniquely identifying a radiation hotspot is sometimes difficult. For example, this situation could occur in a crowded forest (figure 11(b)) because we cannot easily determine whether the tree identified in the optical image is responsible for the hotspot or if a hidden tree causes the hotspot. To resolve such degeneracy, we can use the stereo measurement method to determine the 3-D source position from gamma-ray images taken from two or three different positions (or by multiple cameras) separated by up to 10 meters [18, 19].

Figure 13(a) shows the concept of our 3-D measurement method. By correlating the distribution maps of the same source taken from several locations, we can determine the 3-D position of the source. Figures 13(b) and 13(c) show the simulated resultant images for a single source and for two sources placed up to 5 m apart, respectively. These images were calculated using three distribution maps taken at three different positions with the non-DOI Compton camera. In both the simulation and experiment, we confirmed that the 3-D position, namely the distance to a given hotspot, could be determined within an accuracy of 10−20%.

2014 JINST 9 P11025

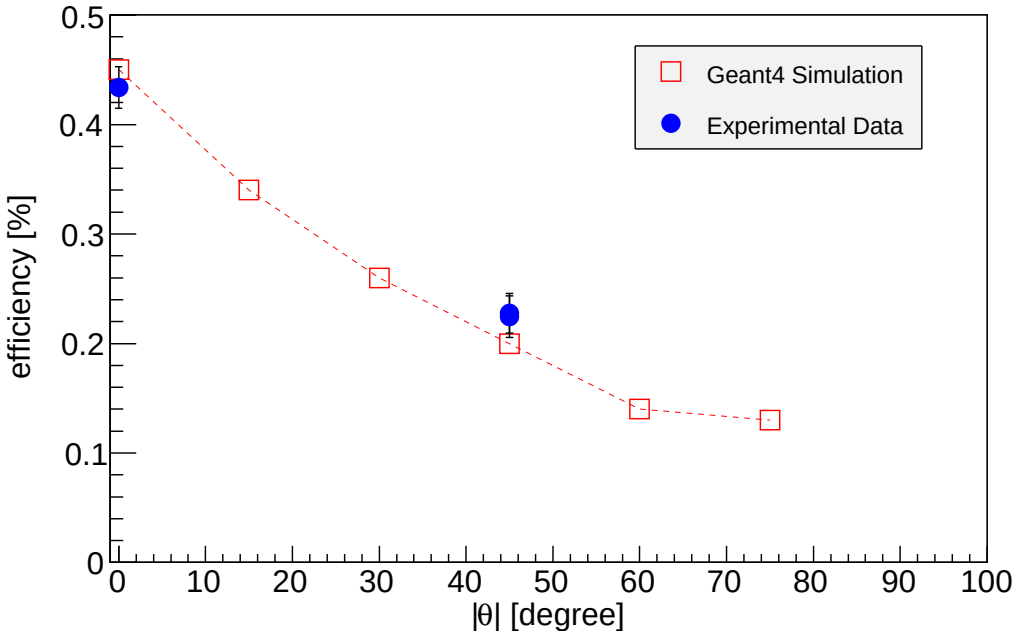

Figure 10. The Geant4 simulation of the intrinsic efficiency of the DOI Compton camera as a function of source position ($|\theta|$). The experimental values agree well with the simulation. The experimental efficiency was $0.43 \pm 0.019\%$ at $\theta = 0^\circ$ and $0.23 \pm 0.018\%/0.22 \pm 0.019\%$ at $\theta = +45^\circ/-45^\circ$.

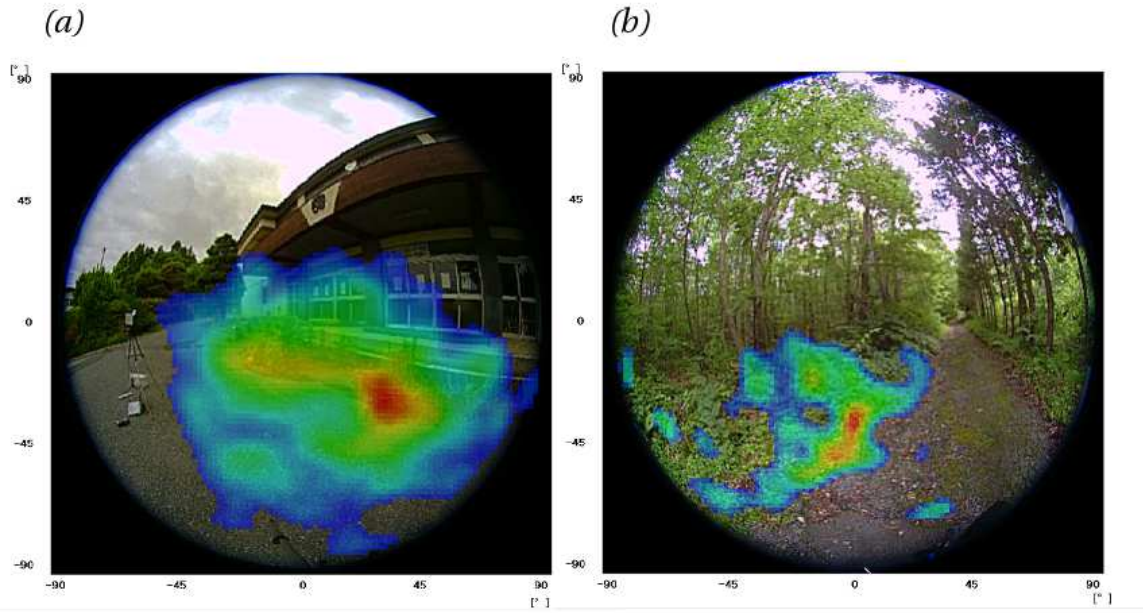

Figure 11. Examples of the SBP images taken in field tests conducted in Fukushima using (a) the non-DOI camera in May 2013 and (b) the DOI camera in July 2014.

2014 JINST 9 P11025

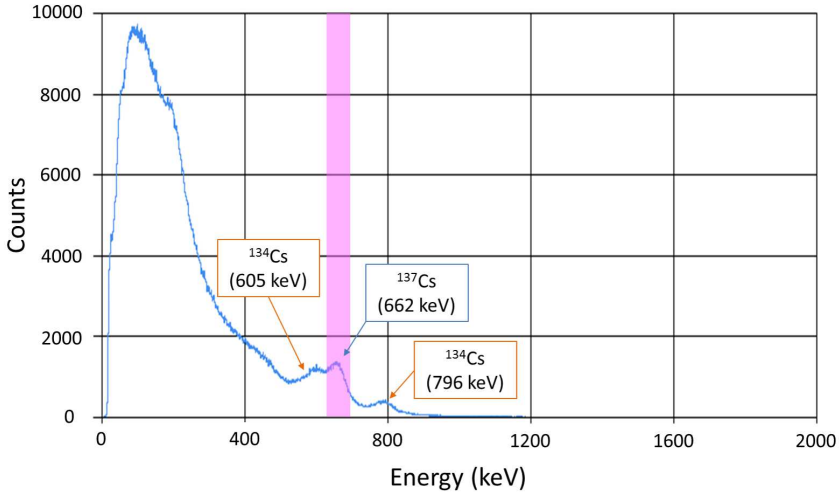

Figure 12. The 1-D energy sum spectrum in field tests conducted in Fukushima, as taken by the DOI Compton camera. The highlighted region represents the energy cut used for image of figure 11(b).

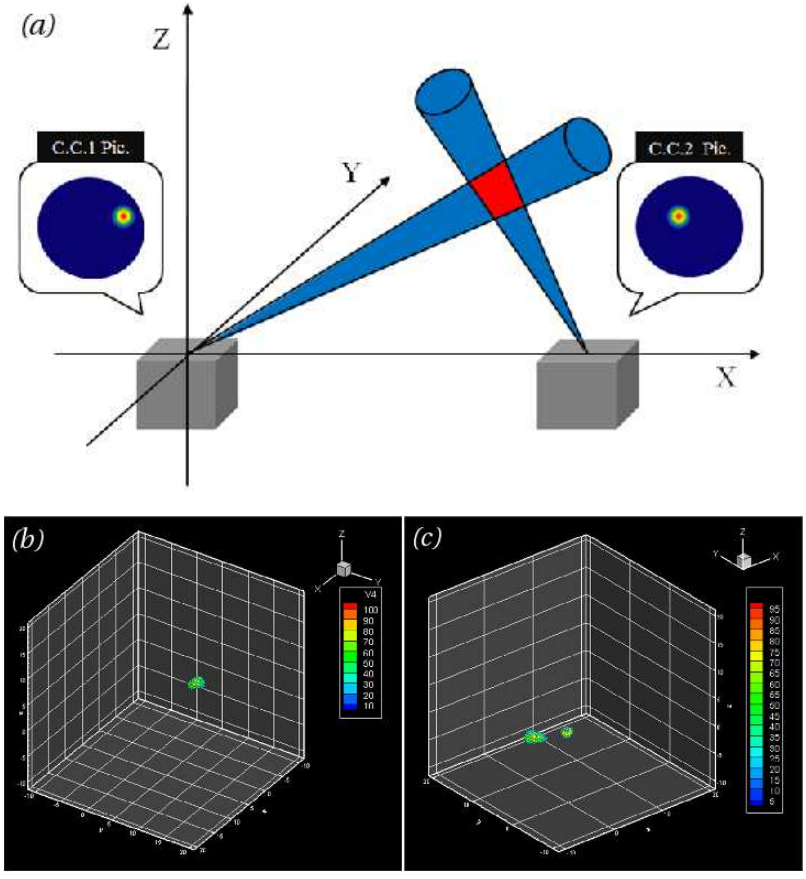

Figure 13. (a) The stereo measurement concept. The 3-D position histogram of (b) a single point source and (c) multiple sources.

2014 JINST 9 P11025

6 Conclusion

In this study, we describe the concept and performance of a novel Compton camera using Ce:GAGG scintillator arrays coupled to MPPC arrays. By employing DOI-capable scintillator arrays, the angular resolution was improved to $\Delta\theta \sim 8^\circ$ (FWHM) at 662 keV from $\Delta\theta \sim 14^\circ$ (FWHM) for the non-DOI camera. The efficiency was also increased by a factor of 1.5–2 as compared to non-DOI due to the use of thicker scintillator arrays. Based on these studies, we conducted a number of field tests in Fukushima using both the non-DOI and DOI Compton cameras. We confirmed that radiation distribution images could typically be collected within a few minutes even under background contamination. Moreover, we also conducted stereo measurements using data from two or more positions, thus enabling 3-D measurements of the radiation distributions.

References

[1] R.W. Todd et al., *A proposed γ camera*, *Nature* **251** (1974) 132.

[2] S. Takeda et al., *Experimental results of the gamma-ray imaging capability with a Si/CdTe semiconductor Compton camera*, *IEEE Trans. Nucl. Sci.* **56** (2009) 783.

[3] H. Tajima et al., *Soft Gamma-ray Detector for the ASTRO-H Mission*, *Proc. SPIE* **7732** (2010) 773216 [arXiv:1010.4997].

[4] S. Motomura et al., *Gamma-Ray Compton Imaging of Multitracer in Biological Samples Using Strip Germanium Telescope*, *IEEE Trans. Nucl. Sci.* **54** (2007) 710.

[5] M.A. Alnaaimi et al., *Performance evaluation of a pixellated Ge Compton camera*, *Phys. Med. Biol.* **56** (2011) 3473.

[6] E.A. Wulf et al., *Germanium Strip Detector Compton Telescope Using Three-Dimensional Readout*, *IEEE Trans. Nucl. Sci.* **50** (2003) 1182.

[7] W. Lee et al., *A compact Compton camera using scintillators for the investigation of nuclear materials*, *Nucl. Instrum. Meth.* **A 624** (2010) 118.

[8] L.E. Sinclair et al., *Simulations of a Scintillator Compton Gamma Imager for Safety and Security*, *IEEE Trans. Nucl. Sci.* **56** (2009) 1262 [arXiv:0809.4240].

[9] J. Kataoka et al., *Handy Compton camera using 3D position-sensitive scintillators coupled with large-area monolithic MPPC arrays*, *Nucl. Instrum. Meth.* **A 732** (2013) 403.

[10] T. Nishiyama et al., *Current Status and Optimization of Handy Compton Camera Using 3D Position-Sensitive Scintillators*, *IEEE Nucl. Sci. Symp. Med. Imag. Conf.* **1** (2013) 1.

[11] H. Suzuki et al., *Gamma-ray visualization module*, *IEEE Nucl. Sci. Symp. Med. Imag. Conf.* **1** (2013) 1.

[12] K. Kamada et al., *Composition engineering in cerium-doped (Lu, Gd)$_3$(Ga, Al)$_5$O$_{12}$ single-crystal scintillators*, *Cryst. Growth Des.* **11** (2011) 4484.

[13] T. Kato et al., *Development of a large-area monolithic 4×4 MPPC array for a future PET scanner employing pixelized Ce:LYSO and Pr:LuAG crystals*, *Nucl. Instrum. Meth.* **A 638** (2011) 83.

[14] T. Kato et al., *A novel gamma-ray detector with submillimeter resolutions using a monolithic MPPC array with pixelized Ce:LYSO and Ce:GGAG crystals*, *Nucl. Instrum. Meth.* **A 699** (2013) 235.

2014 JINST 9 P11025

[15] T. Tsujikawa et al., *Performance of the latest MPPCs with reduced dark counts and improved photon detection efficiency*, *Nucl. Instrum. Meth.* **A 765** (2014) 247.

[16] T. Nakamori et al., *Development of a gamma-ray imager using a large area monolithic* 4×4 *MPPC array for a future PET scanner*, 2012 *JINST* **7** C01083.

[17] A. Kishimoto et al., *Development of a Dual-Sided Readout DOI-PET Module Using Large-Area Monolithic MPPC-Arrays*, *IEEE Trans. Nucl. Sci.* **60** (2013) 38.

[18] K. Takeuchi et al., *Stereo Compton cameras for the 3-D localization of radioactive isotopes optimized by Geant4*, *IEEE Nucl. Sci. Symp. Med. Imag. Conf.* **1** (2013) 1.

[19] K. Takeuchi et al., *"Stereo Compton cameras" for the 3-D locarization of radioisotopes*, *Nucl. Instrum. Meth.* **A 765** (2014) 187.

2014 JINST 9 P11025